Solution of the Dyson equation for nucleons in the superfluid phase

J. Terasaki[a,b], F. Barranco[c], R. A. Broglia[a,b,d], E. Vigezzi[b] and P.F. Bortignon[a,b]

[a] Department of Physics, University of Milan, Via Celoria 16, I-20133 Milan, Italy
[b] INFN Sezione di Milano, Via Celoria 16, I-20133 Milan, Italy
[c] Departamento de Fìsica Aplicada III, Escuela Superior de Ingenieros, Universidad de Sevilla, Camino de los Descubrimientos, Sevilla, Spain
[d] The Niels Bohr Institute, University of Copenhagen, DK-2100 Copenhagen, Denmark

May 23, 2001

Abstract

We investigate the role the interweaving of surface vibrations and nucleon motion has on Cooper pair formation in spherical superfluid nuclei. A quantitative calculation of the state-dependent pairing gap requires to go beyond the quasiparticle approximation, treating in detail the breaking of the single-particle strength and of the associated poles. This is done solving self-consistently the Dyson equation, including both a bare nucleon-nucleon interaction (which for simplicity we choose as a monopole-pairing force of constant matrix elements g) and an induced interaction arizing from the exchange of vibrations (calculated microscopically in QRPA) between pairs of nucleons moving in time reversal states. Both the normal and anomalous density Green functions are included, thus treating self-energy and pairing processes on equal footing. We apply the formalism to the superfluid nucleus ^{120}Sn. Adjusting the value of g so as to reproduce, for levels close to the Fermi level, the empirical odd-even mass difference ($\Delta \approx 1.4$ MeV), it is found that the pairing gap receives about equal contributions from the monopole-pairing force and from the induced interaction. This result is also reflected in the fact that if one were to reproduce the observed Δ allowing the nucleons to interact only through the bare monopole-pairing force, a value of $g \approx 0.233$ MeV ($\approx 28/A$ MeV) is needed, 50% larger than the value $g \approx 0.166$ MeV ($\approx 20/A$ MeV) needed in the full calculation. To keep in mind that the bare and the induced pairing contributions to Δ enter the corresponding equations in a very non-linear fashion. It is furthermore found that self-energy processes reduce the

contribution of the phonon induced interaction to the pairing gap by $\approx 20\%$ as compared to the value obtained by only phonon exchange without taking into account the breaking of the single-particle strength.

PACS codes: 21.30.Fe, 27.60.+j
Keywords: Dyson equation, pairing gap, phonon-induced interaction

1 Introduction

It is well known that single-particle motion in atomic nuclei is strongly renormalized by the coupling to low-lying surface vibrations, which leads to the fragmentation of the single-particle strength and affects basic quantities like the level density at the Fermi surface, the effective mass and the width of giant resonances [1–3]. Recently, it has been shown that the induced interaction resulting from such a coupling (phonon-induced interaction) leads to pairing gaps which account for about half of the experimental values [4]. In what follows we shall refer to these calculations of the state-dependent pairing gap as the Bardeen-Cooper-Schrieffer plus Bloch-Horowitz (BCS+BH) approximation, in keeping with the fact that this form of perturbation theory was used to calculate the induced interaction entering the gap equation and arising from the exchange of phonons between pairs of nucleons moving in time reversal states close to the Fermi level. In these calculations, empirical single-particle levels were used, and the interplay between core polarization and self-energy contributions, as well as the energy-dependence of the effective mass [2] was neglected.

In the present paper we take a step towards a more consistent calculation of the renormalization effects associated with the particle-vibration coupling phenomenon, treating self-energy and induced pairing interaction processes on equal footing (cf. Fig. 1(a)), by solving the Dyson equation (also called Nambu-Gorkov equation, cf. e.g. [5]), describing the motion of nucleons and their contribution to both normal and anomalous densities. Moreover and following ref. [4], we add to this interaction a monopole-pairing force acting on the orbitals close to the Fermi level.

No vertex corrections (cf. e.g. graph (b) of Fig. 1) have been considered in the present calculations, because in the case of ^{120}Sn, the nucleus we use in the present paper to exemplify the theory, vertex correction contributions are found to change (reduce) the value of the state-dependent pairing gap around Fermi level only modestly.[1]

The Dyson equation approach has been customarily used in condensed matter physics to deal with strong coupling superconductors (cf. e.g. ref. [5–9] and refs. therein). In nuclear physics, this scheme has also been used previously both in the

[1] One could argue concerning the validity of the approximation to neglect the vertex correction in terms of Migdal theorem [6,7] which states that the contribution of the vertex renormalization graphs to the total electron-phonon coupling strength is smaller than the lowest-order strength by a factor $\hbar\Omega/E_F$, where $\hbar\Omega$ is a typical phonon energy, E_F being the Fermi energy measured from the bottom of the single-particle potential. Because in the nuclear case $E_F \approx 36$ MeV and $\hbar\Omega$ is of the order of few MeV, the ratio above turns out to be approximately equal to 10^{-1}. However, this estimate can hardly be considered quantitative, because of the marked shell structure displayed by the single-particle levels, and by the associated particle-vibration coupling matrix elements (spin-flip vs. non spin-flip processes) as well as the strong cancellation existing between effective mass and vertex correction contributions associated with core polarization phenomena (cf. e.g. [3]).

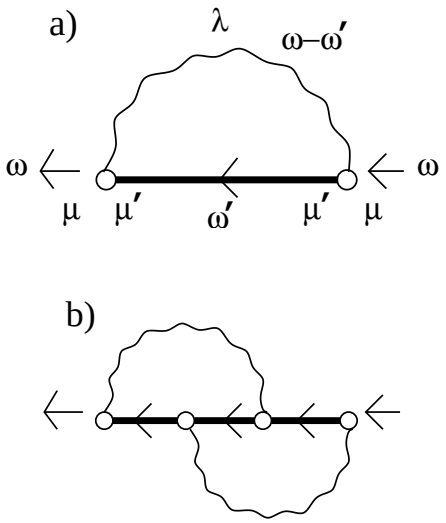

Figure 1. a) The self-energy $\hbar\Sigma_\mu^{\rm pho}(\omega)$ used in the calculations. The wavy line denotes the unperturbed phonon Green function. The heavy arrowed line indicates the perturbed nucleon Green function. The small open circle is the vertex of the particle-phonon interaction. b) Example of self-energy diagram which includes the vertex correction.

case of nuclear matter and of finite nuclei [10–15], the work of ref. [15] being close in spirit to the one discussed here. However in this reference the focus was set on applying the method to correct the phenomenological values of single-particle energies and of the pairing gap to avoid double counting arising in connection with particle-vibration coupling processes. Furthermore, since we do not make use of the linear approximation adopted in that reference to solve the Dyson equation, the present approach should be also able to deal with strong-coupling situations.

In section 2 we present the formalism used in solving the Dyson equation. In section 3 we discuss the results obtained including only the phonon-induced interaction, while in section 4 we add the monopole-pairing force to it. Conclusions are collected in section 5.

2 Solution of the Dyson equation

The core of the present study is the Dyson equation, which for paired systems is written in a matrix form, according to Nambu-Gorkov theory [5]:

$$G_\mu^{-1}(\omega) = G_\mu^{0\,-1}(\omega) - \Sigma_\mu^{\rm pho}(\omega)\ , \tag{1}$$

$$G_\mu(\omega) = \begin{pmatrix} G_\mu^{11}(\omega) & G_\mu^{12}(\omega) \\ G_\mu^{21}(\omega) & G_\mu^{22}(\omega) \end{pmatrix}\ , \tag{2}$$

ω being the energy variable. $G_\mu(\omega)$ denotes the perturbed single-particle (quasiparticle) Green function, and its major poles yield the quasiparticle energies of the system. The diagonal and off-diagonal elements of Eq. (2) are the particle-hole and

the pairing Green function respectively. $G^0_\mu(\omega)$ is the unperturbed single-particle Green function, with elements given by,

$$\frac{1}{\hbar}{G^0_\mu}^{11}(\omega) = \frac{e^{i\eta\omega}}{\omega - (\varepsilon^0_\mu - \varepsilon_F) + i\eta_\mu} \ , \tag{3}$$

$$\frac{1}{\hbar}{G^0_\mu}^{12}(\omega) = \frac{1}{\hbar}{G^0_\mu}^{21}(\omega) = 0 \ , \tag{4}$$

$$\frac{1}{\hbar}{G^0_\mu}^{22}(\omega) = \frac{e^{-i\eta\omega}}{\omega + (\varepsilon^0_\mu - \varepsilon_F) - i\eta_\mu} \ , \tag{5}$$

where ε^0_μ denotes the unperturbed single-particle energy of the single-particle state with quantum numbers μ ($\equiv nlj$). The Fermi level measured from the top of the potential is indicated by ε_F. The parameter η_μ is defined as

$$\eta_\mu = \begin{cases} -\eta \ , & \varepsilon^0_\mu < \varepsilon_{\rm F} \ , \\ \eta \ , & \varepsilon^0_\mu > \varepsilon_{\rm F} \ , \end{cases} \tag{6}$$

where η is real and positive. The self-energy term of the phonon-induced interaction (cf. Fig. 1(a)) is defined as [5],

$$\begin{aligned} \hbar\Sigma^{\rm pho}_\mu(\omega) &= \hbar \begin{pmatrix} \Sigma^{11\,{\rm pho}}_\mu(\omega) & \Sigma^{12\,{\rm pho}}_\mu(\omega) \\ \Sigma^{21\,{\rm pho}}_\mu(\omega) & \Sigma^{22\,{\rm pho}}_\mu(\omega) \end{pmatrix} \\ &= \int_{-\infty}^{\infty} \frac{d\omega'}{2\pi} \sum_{\mu'} \tau_3 \frac{1}{\hbar} G_{\mu'}(\omega')\tau_3 \sum_{\lambda n} \frac{\hbar}{2\Omega_{\lambda n} B_{\lambda n}} \frac{1}{2j_\mu + 1} \\ &\quad \times \left| \langle \mu || R_0 \frac{\partial U}{\partial r} Y_\lambda || \mu' \rangle \right|^2 \frac{i}{\hbar} D^0_{\lambda n}(\omega - \omega') \ , \end{aligned} \tag{7}$$

where $\tau_3 = \begin{pmatrix} 1 & 0 \\ 0 & -1 \end{pmatrix}$. The energy and the inertial parameter of the phonons are denoted by $\hbar\Omega_{\lambda n}$ and by $B_{\lambda n}$, respectively, with the multipolarity λ and an additional index n. The particle-vibration vertex is given by

$$(-)^{j_\mu + j_{\mu'}} \sqrt{\frac{\hbar}{2\Omega_{\lambda n} B_{\lambda n}}} \langle \mu || R_0 \frac{\partial U}{\partial r} Y_\lambda || \mu' \rangle \ , \tag{8}$$

where R_0 and $U(r)$ are the nuclear radius and potential. The phonons are not dressed and are calculated within the QRPA, as was done in ref. [4]. The corresponding (unperturbed) phonon propagator is

$$\frac{i}{\hbar} D^0_{\lambda n}(\omega - \omega') = \frac{i}{\omega - \omega' - \hbar\Omega_{\lambda n} + i\eta_D} + \frac{i}{-\omega + \omega' - \hbar\Omega_{\lambda n} + i\eta_D} \ ,$$

where η_D stands for a real positive parameter.

We solve Eqs. (1) and (7) self-consistently, starting by inserting at the place of $G_{\mu'}$ in Eq. (7) the BCS Green function in an analytical form (see Chap. 7 in [5]), calculating the integral of the self-energy $\Sigma^{\rm pho}_\mu(\omega)$ analytically. The poles $\pm\omega^{\mu m}_{G+}$ (we set ${\rm Re}\,\omega^{\mu m}_{G+} \geq 0$, m being another label distinguishing the pairs of the poles) of the

new Green function are determined by searching, on the real axis, for the roots of the equation[2]

$$\det \overline{G}_{\mu}^{-1}(\pm \mathrm{Re}\, \omega_{G+}^{\mu m}) = 0 \ , \tag{9}$$

where $\overline{G}_{\mu}^{-1}(\omega)$ is calculated from Eq. (1) but neglecting the non-hermitian components:

$$\hbar \overline{G}_{\mu}^{-1}(\omega) = \begin{pmatrix} \omega - \tilde{\varepsilon}_{\mu}^{0} - \mathrm{Re}\, \hbar \Sigma_{\mu}^{11\,\mathrm{pho}}(\omega) & -\hbar \Sigma_{\mu}^{12\,\mathrm{pho}}(\omega) \\ -\hbar \Sigma_{\mu}^{21\,\mathrm{pho}}(\omega) & \omega + \tilde{\varepsilon}_{\mu}^{0} - \mathrm{Re}\, \hbar \Sigma_{\mu}^{22\,\mathrm{pho}}(\omega) \end{pmatrix} \ , \tag{10}$$

with $\tilde{\varepsilon}_{\mu}^{0} = \varepsilon_{\mu}^{0} - \varepsilon_F$. A very small value (1 keV) of the averaging parameters η and η_D is used with an idea to deal with stationary states. The imaginary parameters are so small that we can identify the residue of $\overline{G}_{\mu}^{11}(\omega)/\hbar$ with that of $G_{\mu}^{11}(\omega)/\hbar$, that is,

$$R_{\mu m}^{11}(\pm \omega_{G+}^{\mu m}) \simeq \left(\frac{d}{d\omega} \frac{\hbar}{\overline{G}_{\mu}^{11}(\omega)} \bigg|_{\pm \mathrm{Re}\, \omega_{G+}^{\mu m}} \right)^{-1} \ , \tag{11}$$

where the derivative is taken also on the real axis. $R_{\mu m}^{12}(\pm \omega_{G+}^{\mu m})$ is obtained through a similar equation. The imaginary part of the poles $\pm \omega_{G+}^{\mu m}$ is fixed to be $\mp$ 1 keV for simplicity. Eqs. (9)–(11) are generalizations of those found in Sections 3.4 and 4.3.6 of ref. [2]. The new Green function can now be written as

$$\frac{1}{\hbar} G_{\mu}^{11}(\omega) = \sum_{m} \left(\frac{R_{\mu m}^{11}(\omega_{G+}^{\mu m})}{\omega - \omega_{G+}^{\mu m}} + \frac{R_{\mu m}^{11}(-\omega_{G+}^{\mu m})}{\omega + \omega_{G+}^{\mu m}} \right) e^{i\omega\eta} \ , \tag{12}$$

$$\frac{1}{\hbar} G_{\mu}^{12}(\omega) = \sum_{m} \left(\frac{R_{\mu m}^{12}(\omega_{G+}^{\mu m})}{\omega - \omega_{G+}^{\mu m}} + \frac{R_{\mu m}^{12}(-\omega_{G+}^{\mu m})}{\omega + \omega_{G+}^{\mu m}} \right) \ . \tag{13}$$

Assuming that the ground state of the system is time reversal invariant, the quantities $G_{\mu}^{22}(\omega)$ and $G_{\mu}^{21}(\omega)$ can be written in a similar way in terms of $R_{\mu m}^{11}(\pm \omega_{G+}^{\mu m})$ and $R_{\mu m}^{12\,*}(\pm \omega_{G+}^{\mu m})$, respectively. A new self-energy is then generated, using Eqs. (12) and (13), as

$$\begin{aligned} \hbar \Sigma_{\mu}^{11\,\mathrm{pho}}(\omega) \ = \ & \sum_{\mu' m} \sum_{\lambda n} \frac{\hbar}{2\Omega_{\lambda n} B_{\lambda n}} \left| \langle \mu || R_0 \frac{\partial U}{\partial r} Y_{\lambda} || \mu' \rangle \right|^2 \frac{1}{2j_{\mu} + 1} \\ & \times \left\{ \frac{R_{\mu' m}^{11}(-\omega_{G+}^{\mu' m})}{\omega + \omega_{G+}^{\mu' m} + \hbar\Omega_{\lambda n} - i\eta_D} + \frac{R_{\mu' m}^{11}(\omega_{G+}^{\mu' m})}{\omega - \omega_{G+}^{\mu' m} - \hbar\Omega_{\lambda n} + i\eta_D} \right\} \ . \end{aligned} \tag{14}$$

The other elements can be obtained in a similar way, and the process is iterated until convergence. The Fermi level ε_F is fixed so as to obtain the desired expectation value of the nucleon number

$$\langle \hat{N} \rangle = \sum_{\mu m} (2j_{\mu} + 1)\, R_{\mu m}^{11}(-\omega_{\mathrm{G+}}^{\mu m}) \ . \tag{15}$$

As can be seen From Fig. 1(a) and Eq. (1), this iterative process involves the coupling to an increasingly larger number of phonons at each iteration step. This

[2]We use a mesh of 1 keV, and once the existence of a root is detected in an interval, the bisection method is applied.

in turn enhances the fragmentation of the single-particle strength, leading to an increasingly larger number of poles of the Green function until saturation.[3] For each of the poles $\pm\omega^{\mu m}_{\rm G+}$, the sum $R^{11}_{\mu m}(\omega^{\mu m}_{\rm G+}) + R^{11}_{\mu m}(-\omega^{\mu m}_{\rm G+})$ is interpreted as the single-particle strength of the pole ($R^{11}_{\mu m}(-\omega^{\mu m}_{\rm G+}) = R^{22}_{\mu m}(\omega^{\mu m}_{\rm G+})$). As a rule, and depending on whether pairing correlations are important or not, one or two poles close to ε_F carry most of the single-particle strength in the case of orbitals close to the Fermi level. In particular, in the BCS approximation the two poles $\pm\omega_{\rm G+}$ carry the whole strength, and $R^{11}_{\mu}(\omega^{\mu}_{\rm G+}) + R^{11}_{\mu}(-\omega^{\mu}_{\rm G+}) = u^2_\mu + v^2_\mu = 1$, and $|R^{12}_{\mu}(\pm\omega^{\mu}_{\rm G+})| = u_\mu v_\mu$. In general, however, one needs to take into account more poles, in order to exhaust a substantial fraction of the sum rule

$$\sum_m \left(R^{11}_{\mu m}(\omega^{\mu m}_{\rm G+}) + R^{11}_{\mu m}(-\omega^{\mu m}_{\rm G+}) \right) = 1 \ . \tag{16}$$

We shall label with μm_0 the pole carrying the major single-particle strength, and call it the quasiparticle pole.

3 Induced interaction

We have applied the formalism described above to the calculation of the neutron Green functions of the nucleus ^{120}Sn. In this section we shall concentrate on the phonon-induced interaction, while in the next we shall add the monopole-pairing force with constant matrix elements as a model of the bare neucleon-nucleon force.

The unperturbed single-particle basis ε^0_μ has been calculated with a Woods-Saxon potential using an effective mass $m_k = 0.7m$, m being the bare nucleon mass. With this value, self-energy effects are expected to lead to a sensible single-particle density close to the Fermi level (cf. also Section 4.6.3 in [2]). We have included in the calculation all the single-particle bound levels.

The computation time needed for our calculations depends strongly on the number of phonon modes λn included. The full QRPA response for the multipolarities $\lambda^\pi = 2^+, 3^-, 4^+, 5^-$ in the energy interval 0–20 MeV used in ref. [4] consists of about two hundreds phonon modes of energies $\hbar\Omega_{\lambda n}$ and zero-point amplitudes $\beta_{\lambda n}$ for each multipolarity. We include the four lowest phonons, one for each multipolarity, which give the largest contributions to the induced phonon interaction. We account for the effects of the other roots including only a few effective phonons of energy $\hbar\Omega^{\rm eff}_{\lambda n}$, distributed in the interval 0–20 MeV, choosing their effective strength so that when they are used in the calculation of ref. [4] they reproduce the state-dependent gap obtained there. This is obtained, considering that the sum of the (asymmetrized) matrix elements of the induced interaction between two pairs $(j_\nu)^2_{J=0}, (j_{\nu'})^2_{J=0}$ due to the phonons lying in an energy interval $[\Omega_a, \Omega_b]$, calculated according to the BH formalism, is given by

$$v_{\nu\nu'} = \frac{|\langle\nu'||R_0\frac{\partial U}{\partial r}||\nu\rangle|^2}{(2j_\nu+1)(2j_{\nu'}+1)(2\lambda+1)} \sum_{\Omega_{\lambda n}=\Omega_a}^{\Omega_b} \frac{4\beta^2_{\lambda n}}{E_0 - (e_\nu + e_{\nu'} + \hbar\Omega_{\lambda n})} \ , \tag{17}$$

[3] The number of poles saturates because η and η_D are finite, and we use the mesh method for finding the poles as explained before. That is, the poles with very small residue (strength) are neglected.

Table 1. The energies of the phonon modes $\hbar\Omega_{\lambda n}^{\rm eff}$ and coupling strength $\beta_{\lambda n}^{\rm eff}/\sqrt{2\lambda+1}$. Tables a), b), c) and d) are for $\lambda^\pi = 2^+$, 3^-, 4^+ and 5^-, respectively. The lowest-energy modes ($n = 1$) were taken from a QRPA calculation directly. The coupling strengths as well as the energies of the other modes were determined by the procedure shown in Eqs. (17)–(18).

a)

$\lambda^\pi = 2^+$		
n	$\hbar\Omega_{\lambda n}^{\rm eff}$ [MeV]	$\beta_\lambda^{\rm eff}/\sqrt{2\lambda+1}$
1	1.173	0.0554
2	5.2	0.0134
3	12.5	0.0447

b)

$\lambda^\pi = 3^-$		
n	$\hbar\Omega_{\lambda n}^{\rm eff}$ [MeV]	$\beta_\lambda^{\rm eff}/\sqrt{2\lambda+1}$
1	2.423	0.0591
2	5.57	0.0317
3	10.0	0.0238
4	21.0	0.0291

c)

$\lambda^\pi = 4^+$		
n	$\hbar\Omega_{\lambda n}^{\rm eff}$ [MeV]	$\beta_\lambda^{\rm eff}/\sqrt{2\lambda+1}$
1	2.470	0.0248
2	8.0	0.0300
3	12.0	0.0300
4	15.0	0.0270

d)

$\lambda^\pi = 5^-$		
n	$\hbar\Omega_{\lambda n}^{\rm eff}$ [MeV]	$\beta_\lambda^{\rm eff}/\sqrt{2\lambda+1}$
1	2.402	0.0250
2	8.0	0.0365
3	13.0	0.0166
4	21.0	0.0232

where E_0 and e_ν are the correlation energy of the ground state and the absolute value of the single-particle energy with respect to the Fermi level, respectively. The effective strength of the phonon representing this interval is then chosen so as to satisfy the equations

$$\frac{(\beta_{\lambda n}^{\rm eff})^2}{E_0 - (e_\nu + e_{\nu'} + \hbar\Omega_{\lambda n}^{\rm eff})} = \sum_{\Omega_{\lambda n}=\Omega_a}^{\Omega_b} \frac{\beta_{\lambda n}^2}{E_0 - (e_\nu + e_{\nu'} + \hbar\Omega_{\lambda n})} \ , \tag{18a}$$

$$\hbar\Omega_{\lambda n}^{\rm eff} = \hbar\Omega_b \ , \tag{18b}$$

for the pairs $(j_\nu)^2_{J=0}, (j_{\nu'})^2_{J=0}$ giving the largest contribution to the pairing gap for the multipolarity λ. The energies and zero-point amplitudes devided by $\sqrt{2\lambda+1}$ of the effective phonons are listed in Table 1. Then the coupling strength

$$\frac{\hbar}{2\Omega_{\lambda n}^{\rm eff} B_{\lambda n}^{\rm eff}} = \frac{(\beta_{\lambda n}^{\rm eff})^2}{2\lambda+1} \ ,$$

is used for Eq. (14). The BCS+BH calculation performed with this restricted ensemble of phonons reproduces the state-dependent pairing gaps of ref. [4] within a few per cent.

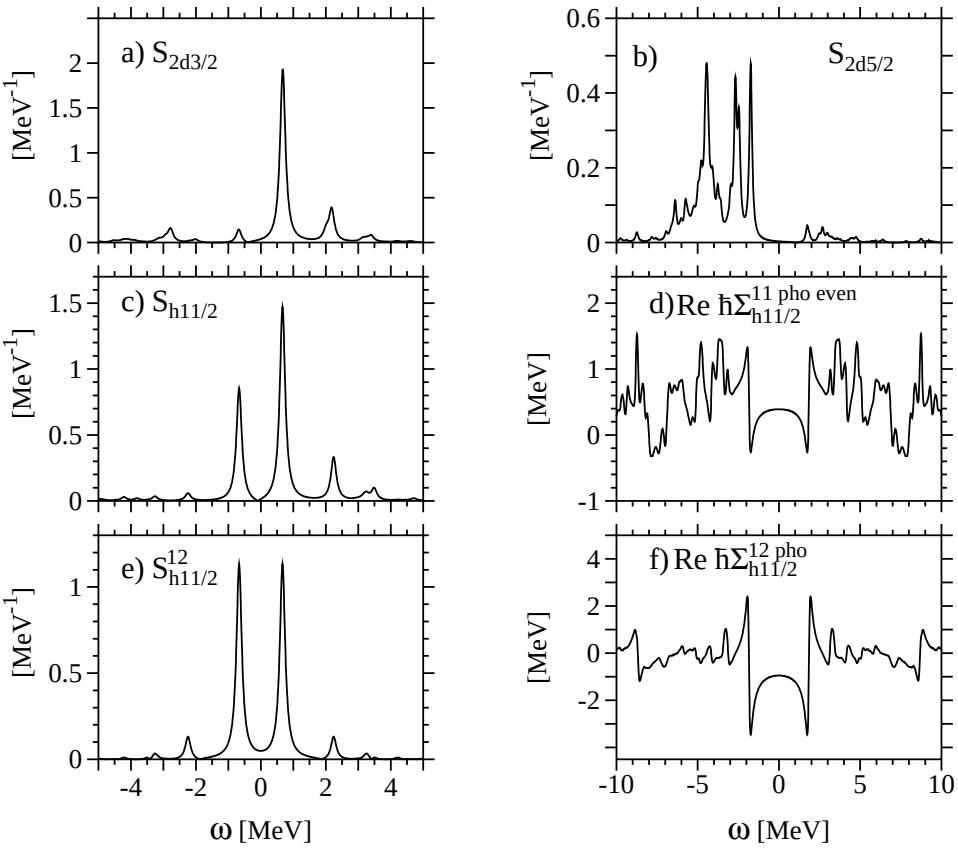

Figure 2. a) The spectral function of $2d_{3/2}$ calculated using the poles and residues of the solution of the Dyson equation. To display the results in terms of a smooth continuous curve, the results have been folded with a smooth function with FWHM of 0.1 MeV. Similar foldings have been performed in connection with the other plots. b) Same but for the $2d_{5/2}$ orbital , c) The spectral function of the $1h_{11/2}$ orbital, d) The even self-energy of the $1h_{11/2}$ orbital (real part), e) The pairing spectral function calculated in a similar way as the spectral function, f) The pairing self-energy (real part).

Because the number of the poles can vary from one iteration step to the next, the solution displays (small) fluctuations. We obtained a reasonable accuracy in the particle number $\langle \hat{N} \rangle = 70 \pm 0.1$ and negligible fluctuations in the perturbed single-particle levels and the state-dependent pairing gaps (definitions are given later) for most of the orbitals. The sum of the single-particle strength for a given orbital μ is as a rule larger than 0.90 in the valence shell.[4]

[4] To be noted that of all the (hundreds or eventually thousands) poles, only a fraction ($\leq 10-20$) carry an appreciable single-particle strength for orbitals near the Fermi level. Consequently, calculations made considering only these poles explicitly lead to results which coincide within 10%, with the results of the more accurate calculation presented in this paper.

The spectral function

$$S_\mu(\omega) = \frac{1}{\pi\hbar}|\mathrm{Im}\, G^{11}_\mu(\omega)| \ , \tag{19}$$

of some levels is shown in Fig. 2 (graphs (a),(b) and (c)). From this figure it can be seen that the quasiparticle approximation (keeping only one (no pairing) or two (with pairing) pole(s)) works well for the level $2d_{3/2}$, (particle-like quasiparticle, cf. Fig. 2(a)), and $1h_{11/2}$ (with an associated single-particle strength $R^{11}_{\mu m_0}(-\omega^{\mu m_0}_{G+}) \approx 0.3$, cf. Fig. 2(c)), but breaks down for the hole-like $2d_{5/2}$ level (cf. Fig. 2(b)), which displays a substantial degree of fragmentation, because one of the poles of $2d_{5/2}$ is almost degenerate with the $1h_{11/2} \times 3^-$ state, then the single-particle strength (residue) of the pole becomes small (see Eqs. (14), (1) and (11)), and the other poles carry more strength. In addition, a large matrix element connecting $1h_{11/2}$ and $2d_{5/2}$ with $\lambda^\pi\, n = 3^-\, 1$ (see Eq. (8)) enhances the fragmentation. Besides the spectral function, we also display in Fig. 2 the even self-energy

$$\hbar\Sigma^{11\mathrm{pho}^{\mathrm{even}}}_\mu(\omega) = \frac{\hbar}{2}\Big(\Sigma^{11\mathrm{pho}}_\mu(\omega) + \Sigma^{11\mathrm{pho}}_\mu(-\omega)\Big) \ . \tag{20}$$

This is shown in Fig. 2(d) for $\mu = 1h_{11/2}$. Its value calculated at the quasiparticle peak of the spectral function gives the approximate energy of the renormalized single-particle spectra

$$\varepsilon^1_\mu = \frac{1}{Z_\mu(\omega^{\mu m_0}_{\mathrm{G}+})}\Big(\tilde{\varepsilon}^0_\mu + \hbar\mathrm{Re}\,\Sigma^{11\mathrm{pho}^{\mathrm{even}}}_\mu(\omega^{\mu m_0}_{G+})\Big) + \varepsilon_F \ , \tag{21}$$

with

$$Z_\mu(\omega^{\mu m}_{\mathrm{G}+}) = 1 - \frac{\hbar\mathrm{Re}\,\Sigma^{11\mathrm{pho}^{\mathrm{odd}}}_\mu(\omega^{\mu m}_{\mathrm{G}+})}{\mathrm{Re}\,\omega^{\mu m}_{\mathrm{G}+}} \ .$$

The function $\hbar\Sigma^{11\mathrm{pho}^{\mathrm{odd}}}_\mu(\omega^{\mu m}_{\mathrm{G}+})$ is the odd component of the self-energy. (See Chap. 7 in ref. [5] in connection to $Z_\mu(\omega^{\mu m}_{G+})$.)

The original single-particle spectrum is compared in Fig. 3(a) with the energies ε^1_μ of the main (quasiparticle) peaks. It is seen that the self-energy processes increase the level density in the valence shell. This increase is essentially due to the rise of the energy of the hole states.

The spectral function and self-energy shown above have their counterpart in the pairing channel. The pairing spectral function $S^{12}_\mu(\omega)$ corresponds to the anomalous density. In the BCS limit it is peaked at the quasiparticle energy and corresponds to the product $u_\mu v_\mu$. The function $S^{12}_\mu(\omega)$ is shown in Fig. 2(e) for $\mu = 1h_{11/2}$. The pairing self-energy $\hbar\Sigma^{12\mathrm{pho}}_\mu(\omega)$ is shown in Fig. 2(f), again for the level $\mu = 1h_{11/2}$. The complex state-dependent gaps are given by [5]

$$\Delta^{\mathrm{pho}}_\mu = \frac{\hbar\Sigma^{12\mathrm{pho}}_\mu(\omega^{\mu m_0}_{\mathrm{G}+})}{Z_\mu(\omega^{\mu m_0}_{\mathrm{G}+})} \ . \tag{22}$$

The assignment of a state-dependent pairing gap as well as a perturbed single-particle energy is valid only to the extent that the quasiparticle approximation is valid, thus the assignment may not be adequate for the single-particle orbital $d_{5/2}$

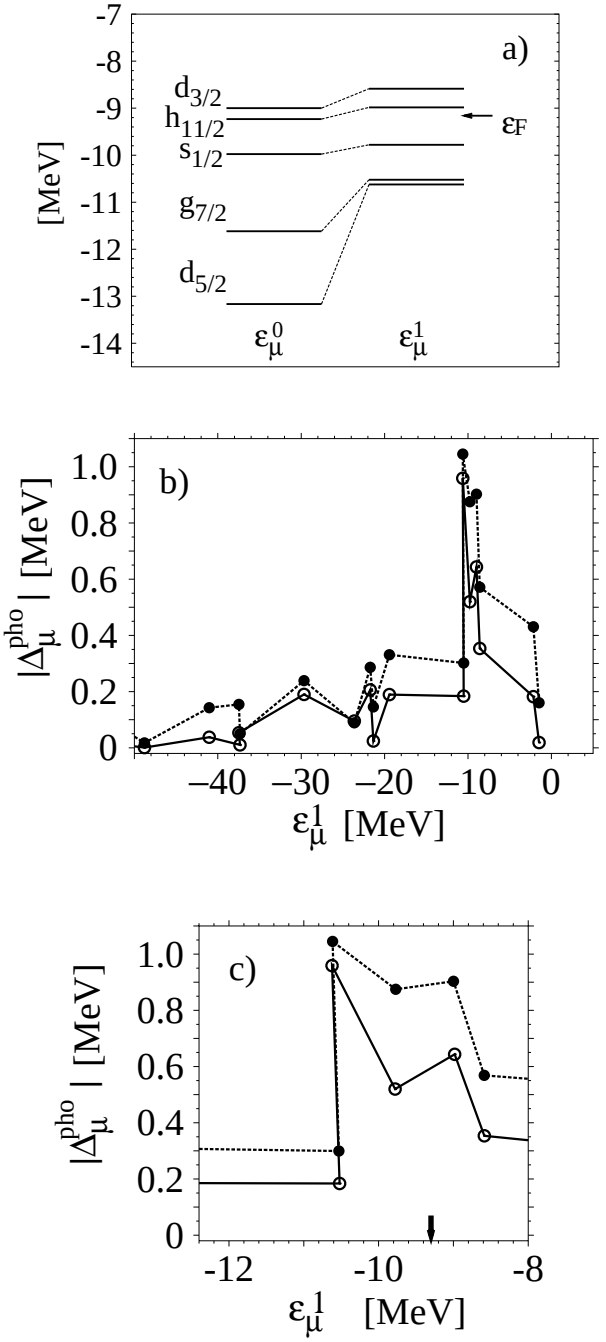

Figure 3. a) The unperturbed single-particle levels ε^0_μ near the Fermi level ε_F and the perturbed levels ε^1_μ corresponding to the quasiparticle poles. b) The state-dependent pairing gaps corresponding to the quasiparticle poles (open circles) and the gaps of the BCS+BH calculation (filled circles) as a function of the renormalized (perturbed) single-particle energies ε^1_μ. c) A magnification of (b) near the Fermi level ε_F. The arrow indicates the Fermi level associated with the Dyson calculation.

(cf. Fig. 2(b)), which is strongly fragmented. In this case, a tentative quasiparticle pole (the right major peak in Fig. 2(b)) was used. The results of the calculation are collected in Table 2, and the gaps associated to the quasiparticle peaks $\omega_{\mathrm{G}+}^{\mu m_0}$ are shown in Figs. 3(b) and (c) in absolute value, where they are compared with the pairing gaps in the BCS+BH approximation calculated using Table 1 and the renormalized (perturbed) single-particle spectra ε_μ^1 of the Dyson calculation (these energies were used for calculating e_ν in Eqs. (17) and (18a). Close to the Fermi level, see Fig. 3(c), the gaps of Dyson calculation are systematically lower; differences of up to 400 keV between the two calculations are observed. In average in the valence shell, the difference is ~ 200 keV.

It is also interesting to calculate more global quantities, like e.g. the pairing correlation energy. Within the framework of the Dyson equation, the contribution to the total ground state energy of the system arising from pairing correlations is

$$\begin{aligned} E_{\mathrm{pair}}^{\mathrm{pho}} &= -i\sum_\mu (2j_\mu+1)\frac{1}{2}\int_{-\infty}^{\infty}\frac{d\omega}{2\pi}\Big(\hbar\Sigma_\mu^{12\,\mathrm{pho}}(\omega)\frac{1}{\hbar}G_\mu^{21}(\omega)e^{i\eta\omega} \\ &\quad + \hbar\Sigma_\mu^{21\,\mathrm{pho}}(\omega)\frac{1}{\hbar}G_\mu^{12}(\omega)e^{-i\eta\omega}\Big)\ , \end{aligned} \tag{23}$$

in keeping with the fact that the quantities entering the above equation are the only ones depending explicitly on the anomalous density. In the case of ^{120}Sn, $E_{\mathrm{pair}}^{\mathrm{pho}} = -3.9$ MeV, a number to be compared with $E_{\mathrm{pair}}(\mathrm{BCS+BH}) = -4.6$ MeV calculated making use of the BCS relation

$$E_{\mathrm{pair}}(\mathrm{BCS+BH}) = -\sum_\mu \frac{2j_\mu+1}{2}u_\mu v_\mu \Delta_\mu(\mathrm{BCS+BH})\ , \tag{24}$$

where $\Delta_\mu(\mathrm{BCS+BH})$ is the pairing gap calculated in the BCS+BH approximation.

We have also performed calculations using only two phonons, corresponding to the low-lying $\lambda^\pi = 2^+$ and 3^- modes ($n = 1$ in Table 1). The resulting average value of the pairing gap in the valence shell is 0.29 MeV, which represents about 50% of the value (0.54 MeV) obtained using all the effective phonons listed in Table 1. It is seen that, while the low-lying phonons give the largest contribution to the induced pairing gap, the inclusion of the other modes increases the gap further.

The perturbed single-particle levels in the valence shell in the calculation using only the low-lying 2^+ and 3^- modes are less compressed around the Fermi level by only 100 keV in average as compared to those obtained in the full calculation, thus the perturbed spectrum is similar to Fig. 3(a).

4 Induced plus monopole interaction

The results presented in the previous section included only the contribution of the phonon induced interaction. However, a realistic calculation of pairing correlations must include also a bare nucleon-nucleon interaction. We do this in the present section, adding to the self-energy of the phonon induced interaction used above (cf. Eq. (7)) the standard monopole (seniority) pairing field acting in the valence shell (v.s.). Associated self-energy reads

$$\hbar\Sigma_\mu^{12\,P0} = \hbar\Sigma_\mu^{21\,P0\,*}$$

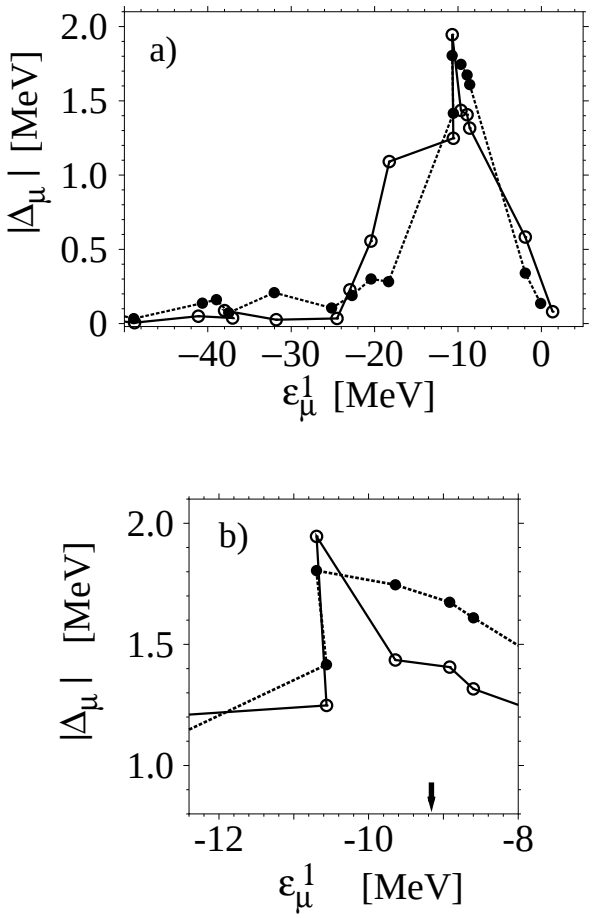

Figure 4. a) The pairing gaps obtained solving the Dyson equation including the monopole+induced interaction (open circles) are compared with the corresponding BCS+BH calculation (filled circles). b) A magnification of (a) near the Fermi level indicated by the arrow.

$$= \begin{cases} -\dfrac{g}{2} \displaystyle\sum_{\mu' \in \text{v.s.},\, m} (2j_{\mu'}+1)\, R^{12}_{\mu' m}(-\omega^{\mu' m}_{G+}) \ , & \text{for } \mu \text{ in v.s. ,} \\ 0 \ , & \text{for other } \mu \ , \end{cases} \tag{25}$$

$$\hbar\Sigma^{11\,P0}_\mu = \hbar\Sigma^{22\,P0}_\mu = 0 \ . \tag{26}$$

The experimental value of the pairing gap, deduced from the experimental odd-even mass difference, is $\Delta \simeq 1.4$ MeV (cf. Chap. 2 in [17]). The state-dependent gap obtained using $g = 20/A = 0.166$ MeV, plus the induced phonon interaction used in the previous section, is shown in Fig. 4; the average pairing gap in the valence shell 1.46 MeV is close to the experimental value. The strength $g = 0.166$ MeV should be compared with the value $g = 28/A = 0.233$ MeV needed to obtain the experimental value using the monopole-pairing field (25) and (26) without any phonon coupling (that is, performing a simple BCS calculation starting from the unperturbed single-particle spectrum with $m^* = 0.7m$).

The enhancement of the pairing gap due to the induced phonon interaction seems to be in contrast with the effect of the induced interaction in nuclear matter, where it usually decreases the pairing gap[5]. In fact, in neutron matter the induced interaction takes place mostly through the exchange of $S = 1$ excitations via the spin-spin part, $(\boldsymbol{s}_1 \cdot \boldsymbol{s}_2)V_s$, of the nucleon-nucleon force, which leads to a repulsive interaction, and tends to suppress the pairing gap. In the case of finite nuclei the absence of collectivity associated to the $S = 1$ modes should make its contribution only marginal with respect to the effect of the strongly collective low-lying surface modes treated in this paper.

In order to get more insight in the result shown in Fig. 4, we decompose the anomalous self-energy Σ^{12}_μ in the sum of two terms, including only the matrix elements of either the induced or the monopole interaction,

$$\hbar\Sigma^{12}_\mu(\omega^{\mu m_0}_{G+}) = \hbar\Sigma^{12\mathrm{pho}}_\mu(\omega^{\mu m_0}_{G+}) + \hbar\Sigma^{12P0}_\mu \ . \tag{27}$$

The imaginary parts of $\hbar\Sigma^{12\mathrm{pho}}_\mu(\omega^{\mu m_0}_{G+})$ and $\hbar\Sigma^{12P0}_\mu$ are negligible, and the real parts have the same sign. Also the state-dependent pairing gap, defined as

$$\Delta_\mu = \frac{\hbar\Sigma^{12}_\mu(\omega^{\mu m_0}_{G+})}{Z_\mu(\omega^{\mu m_0}_{G+})} \ , \tag{28}$$

can then be separated into two contributions,

$$\Delta_\mu = \Delta^{\mathrm{pho}}_\mu + \Delta^{P0}_\mu \ , \tag{29}$$

with

$$\Delta^{P0}_\mu = \frac{\hbar\Sigma^{12P0}_\mu}{Z_\mu(\omega^{\mu m_0}_{G+})} \ .$$

The monopole interaction has only a small effect on the values of Z_μ, since the interaction does not act in the particle-hole channel: from Tables 2 and 3 it can be seen that the values of Z_μ obtained with or without the monopole interaction agree within 10% for all the valence orbitals. From Table 3 it can also be seen that the pairing gaps Δ_μ receive similar contributions from $\Delta^{\mathrm{pho}}_\mu$ and from Δ^{P0}_μ, except for the fragmented level $d_{5/2}$ where the phonon gap is much larger. In particular, the values of $\Delta^{\mathrm{pho}}_\mu$ are enhanced compared to those obtained in section 3 without the monopole interaction, and listed in Table 2.

Finally, in Fig. 4 we compare the gaps obtained in the present calculations with a BCS+BH calculation of the kind performed in [4], but including the same monopole interaction and the same effective particle-vibration couplings as used here. It is seen that the Dyson calculation leads to gaps which are lower again by about 200 keV in average in the valence shell as compared to the BCS+BH results. This is because nucleons spend, in the Dyson scheme, part of their time in more complicated configurations.

[5] It was shown in ref. [16] that the sign of the polarization effect is density dependent in nuclear matter and that the effect reduces the gap at low densities.

Table 2. The result for the orbitals in the valence shell of the Dyson calculation with only the phonon-induced interaction including the effective coupling strengths. Only the real parts of the gaps are shown, since the imaginary parts are negligible. $\hbar\Sigma_\mu^{12\mathrm{pho}}$ denotes the value at the quasiparticle pole $\hbar\Sigma_\mu^{12\mathrm{pho}}(\omega_{G+}^{\mu m_0})$.

	ε_μ^0 [MeV]	$\Delta_\mu^{\mathrm{pho}}$ [MeV]	$\hbar\Sigma_\mu^{12\mathrm{pho}}$ [MeV]	Z_μ
$h_{11/2}$	−9.232	−0.642	−1.049	1.63
$d_{5/2}$	−13.166	−0.951	−2.396	2.52
$s_{1/2}$	−9.977	−0.519	−0.866	1.67
$g_{7/2}$	−11.618	−0.183	−0.231	1.26
$d_{3/2}$	−9.000	−0.353	−0.578	1.64

Table 3. The result of the Dyson calculation with both the phonon-induced interaction, including the effective coupling strengths, and the monopole (seniority) pairing force. For the notations, see the text. Note that $\hbar\Sigma_\mu^{12\mathrm{pho}}$, and Z_μ are abbreviations of $\hbar\Sigma_\mu^{12\mathrm{pho}}(\omega_{G+}^{\mu m_0})$, and $Z_\mu(\omega_{G+}^{\mu m_0})$, respectively. Again we show the real parts of the pairing gaps.

	Δ_μ [MeV]	$\Delta_\mu^{\mathrm{pho}}$ [MeV]	$\hbar\Sigma_\mu^{12\mathrm{pho}}$ [MeV]	Δ_μ^{P0} [MeV]	$\hbar\Sigma_\mu^{12P0}$ [MeV]	Z_μ
$h_{11/2}$	−1.400	−0.868	−1.287	−0.531	−0.788	1.48
$d_{5/2}$	−1.942	−1.602	−3.710	−0.340	−0.788	2.32
$s_{1/2}$	−1.429	−0.919	−1.419	−0.510	−0.788	1.54
$g_{7/2}$	−1.244	−0.677	−0.942	−0.566	−0.788	1.39
$d_{3/2}$	−1.311	−0.792	−1.204	−0.518	−0.788	1.52

5 Conclusions

One can conclude, that in the case studied the induced phonon interaction contributes substantially to pairing correlations: the strength of the monopole interaction, needed to obtain the experimental value of the pairing gap, is strongly reduced when the phonon contribution is included, as the gaps receive almost equal contributions from the monopole and from the induced interaction.

It is also seen that a quantitative estimate of the pairing induced interaction requires a self-consistent treatment of the particle-vibration renormalization processes, as the one performed here solving the Dyson equation. In fact the self-consistent treatment lowers the gaps by about 20% as compared to the empirical treatment of the effective mass processes, which does not include a detailed description of the breaking of single-particle strength.

References

[1] A. Bohr and B. R. Mottelson, Nuclear Structure, Vol II, W. A. Benjamin, Reading, 1975.

[2] C. Mahaux, P. F. Bortignon, R. A. Broglia and C. H. Dasso, Phys. Rep. **120** (1985) 1.

[3] P. F. Bortignon, A. Bracco and R. A. Broglia, Giant resonances. Nuclear structure at finite temperature, Harwood Academic Press, New York, 1998.

[4] F. Barranco, R. A. Broglia , G. Gori, V. Vigezzi, P. F. Bortignon and J. Terasaki, Phys. Rev. Lett. **83** (1999) 2147

[5] J. R. Schrieffer, Theory of Superconductivity, Addison-Wesley, Redwood City, 1964.

[6] A. B. Migdal, Sov. Phys. JETP **7** (1958) 996

[7] G. Grimvall, The electron-phonon interaction in metals, North-Holland, Amsterdam, 1981.

[8] P. B. Allen and B. Mitrović, in: H. Ehrenreich, F. Seitz and D. Turnbull (Eds.), Solid State Physics, Vol 37, Academic press, New York, 1982, p. 1

[9] D. J. Scalapino, in: R. D. Parks (Ed.), Superconductivity, Vol I, M. Dekker Inc., New York, 1969, p. 449.

[10] M. Baldo and A. Grasso, Phys. Lett. **B485** (2000) 115

[11] P. Bożek, Nucl. Phys. **A657** (1999) 187

[12] D. Van Neck, M. Waroquier, J. Ryckebusch, Nucl. Phys. **A530** (1991) 347.

[13] V. Van der Sluys, D. Van Neck, M. Waroquier and J. Ryckebusch, Nucl. Phys. **A551** (1993) 210

[14] H. Müther and L. D. Skouras, Nucl. Phys. **A581** (1995) 247.

[15] A. V. Avdeenkov and S. P. Kamerdzhiev, Phys. Atom. Nucl. **62** (1999) 563; Phys. Lett. **B459** (1999) 423.

[16] H.-J. Schulze, J. Cugnon, A. Lejeune, M. Baldo and U. Lombardo, Phys. Lett. **B375** (1996) 1.

[17] A. Bohr and B. R. Mottelson, Nuclear Structure, Vol I, New York, Benjamin, 1969.